Highlighting the need for high-speed imaging in capillary breakup extensional rheometry

OPEN ACCESS
IOP Publishing
Measurement Science and Technology
Meas. Sci. Technol. **32** (2021) 095301 (8pp)
https://doi.org/10.1088/1361-6501/abeea8

Highlighting the need for high-speed imaging in capillary breakup extensional rheometry

Henry C-H Ng* and **Robert J Poole**

School of Engineering, University of Liverpool, Brownlow Hill, Liverpool L69 3GH, United Kingdom

E-mail: hchng@liverpool.ac.uk and hchng@liverpool.ac.uk

Received 28 December 2020, revised 9 March 2021
Accepted for publication 15 March 2021
Published 28 May 2021

Abstract

The capillary breakup extensional rheometer is commonly used to determine material properties of complex fluids. This is achieved by tracking the diameter evolution of a liquid bridge undergoing capillary thinning and breakup in a uniaxial extensional flow. Typically, the filament diameter evolution is tracked at the mid-plane between the two end-plates using a laser micrometer. We show using high-speed imaging that while this arrangement is satisfactory in flows where the filament is long (relative to its initial diameter), slender and approximately cylindrical, errors can be significant when the filaments are short (and with a non-negligible curvature) such as encountered when using the so-called slow-retraction-method and 'Dripping-onto-Substrate' rheometry. We will further highlight the need for high-speed imaging in CaBER experiments by considering errors induced when the laser micrometer is misaligned with the location of filament breakup. This latter source of error will be particularly relevant for capillary breakup experiments where the location of filament breakup is not typically known *a priori*, such as the case for many so-called 'yield-stress' fluids.

Keywords: rheometer, extensional rheometry, uniaxial flow, capillary breakup extensional rheometer

(Some figures may appear in colour only in the online journal)

1. Introduction

Filament-thinning or 'capillary breakup extensional rheometry' (HAAKE™ CaBER™ 1 sold as a commercial device by Thermo Scientific™) is commonly used to extract the extensional properties of fluids [1, 2] such as the apparent extensional viscosity, $\eta_{\mathrm{app,ext}}(\dot{\varepsilon})$, the critical time to breakup, t_c, and fluid relaxation time (or, more accurately, a 'characteristic time for extensional stress growth' as the stress is growing rather than relaxing). In these experiments, an unstable fluid filament ('unstable' in the sense that surface tension is acting to rupture it) is set up between two parallel end-plates. After an initial deformation, i.e. stretching, the fluid filament undergoes capillary thinning with an approximately uniaxial extensional flow subsequently developing. Tracking the time evolution of the filament radius as it undergoes self-thinning allows the user to obtain material properties from CaBER measurements. These properties are often transient quantities and expressed as a function of time t, or more appropriately, strain rate $\dot{\varepsilon}$. The strain rate of the fluid filament is given by

$$\dot{\varepsilon} = -\frac{2}{R_{\mathrm{mid}}(t)}\frac{dR_{\mathrm{mid}}(t)}{dt} \tag{1}$$

where R_{mid} is the filament radius at mid-height. In the absence of inertia, the fluid filament selects a self-similar force balance between visco-(elasto) stresses and capillary pressure [3] and

* Author to whom any correspondence should be addressed.

the apparent extensional viscosity can theoretically be determined from [4]:

$$\eta_{\text{app,ext}} = \frac{\sigma/R_{\text{mid}}(t)}{\dot{\varepsilon}} = \frac{\sigma}{2dR_{\text{mid}}(t)/dt}, \tag{2}$$

where σ represents surface tension. Equation (2) arises from a force-balance that assumes an ideal, axially uniform thread [5]. In practice, however, the filaments set up in CaBER measurements, while slender, are generally, not uniform [2]. With an appropriate correction factor X, the apparent extensional viscosity, $\eta_{\text{app,ext}}$, can be obtained from

$$\eta_{\text{app,ext}} = \frac{(2X-1)\sigma}{2dR_{\text{mid}}(t)/dt} \tag{3}$$

where it has been shown in simulations [3] and experiments [2] that $X = 0.7127$ for viscous Newtonian filaments. We are also able to estimate a Hencky strain ε from the filament radius evolution profiles according to

$$\epsilon = 2\log\left(\frac{R_0}{R(t)}\right), \tag{4}$$

where R_0 is the filament initial radius.

In experiments, the filament-thinning evolution is typically tracked using a laser micrometer [6–19] (such as that originally equipped on the commercial HAAKE™ CaBER™ 1 device) or high-speed imaging techniques. Typically, the laser micrometer has a finite thickness $h_{\text{micro}} = O(1\text{ mm})$ and, in the case of the commercial HAAKE™ CaBER™ 1 device, its axial location is fixed, and it is the position of the end-plates that is adjusted to ensure that the laser micrometer is located at the axial location of filament breakup.

High-speed imaging techniques deployed in CaBER experiments are particularly relevant for probing fluids of ultra-short relaxation times [20] and for instances when the axial location of filament breakup is not known *a priori* which is often the case for so-called yield-stress fluids [21, 22] and suspensions which exhibit localised necking [23, 24]. When probing fluids of ultra-short relaxation times, the formed filament lengths are generally short (relative to its initial diameter) regardless of the measurement protocol employed. In order to observe filament-thinning when using the standard step-stretch protocol, the final filament height is limited by the requirement that the stretching time must be shorter than the filament breakup time [25] such that the filaments are typically kept short in order to avoid applying excessive plate separation velocities that in turn introduce inertia [26]. As an alternative to the step-stretch method, Campo-Deaño and Clasen [27] introduced the slow-retraction-method (SRM), a modified CaBER operating protocol where the fluid between the end-plates is first brought to its static stability limit and then pushed beyond that limit by inducing plate separation at very low velocities. The SRM significantly reduces inertia (relative to the standard step-stretch technique) and reportedly extends the operating window of the HAAKE™ CaBER™ 1 to viscosities as low as $\eta = 27$ mPa s, while resolving relaxation times as low as $\lambda = 240$ µs. The recently developed dripping-onto-substrate (DoS) rheometry technique [28, 29], where a filament is formed between a sessile drop and a nozzle by dripping the test material onto a substrate, further extends the operating window of capillary breakup extensional rheomerty to fluid viscosities as low as $\eta = 1$ mPa s [30, 31] with relaxation times of $\lambda = 20$ µs [32] being resolvable.

In practice, most if not all studies that utilize the SRM and DoS techniques rely on high-speed imaging to observe the capillary thinning and breakup dynamics of low viscosity fluids although, in theory, a laser micrometer could still be used to extract the filament-thinning profiles (given that it has a high enough sampling rate). In this paper, we will further highlight the need for high-speed imaging in capillary breakup rheometry experiments by explicitly considering two sources of error induced by using the laser micrometer to track the filament radius evolution. First, we will consider the error owing to averaging the filament-thinning evolution profile over a finite thickness. Second, we outline the error induced when material properties are extracted from filament-thinning profiles that are not aligned with the axial location of ultimate breakup. To assess these errors, we employ a 'virtual' laser micrometer by extracting horizontal pixel lines from high-speed images of capillary breakup extensional rheometry experiments.

2. Experimental setup

Our capillary-thinning experiments were carried out on a commercial HAAKE™ CaBER™ 1 equipped with end-plates of radius $R_p = 2$ mm which were set to an initial gap of $L_0 = 2$ mm. The initial gap between the end-plates was set by manually traversing the bottom plate with a micrometer (Holex T0503-100A 0–25 mm, Resolution 0.002 mm) and then positioning the top plate with the CaBER device's motor drive. During the experiments the bottom plate remains stationary and the top plate is pulled upwards at a constant velocity.

Images of the fluid filaments undergoing capillary thinning and breakup were captured using an IDT XS5-M-4 high-speed camera (Integrated Design Tools, Inc. USA, 1280×1024) and viewed through a microscope objective and extension tube combination which yielded a spatial resolution of 1.97 µm pixel^{-1} at maximum magnification of 6×. The filaments were backlit using a ThorLabs OSL2 FiberIlluminator to aid in the detection of the air/fluid interface in image processing. To increase the camera acquisition rate to 6040 frames per second, the region of interest was reduced to 1280×176 pixels which limited the field-of-view to 2.52×0.35 mm (height-by-width) at maximum magnification. As a result, the evolution of the filament radius $R(x)$ (where x is the axial direction along the filament axis) is only imaged for the latter stages of thinning and ultimate breakup.

The filament image sequences were processed in MATLAB® using bespoke routines developed in house. A threshold was employed to maximize the contrast at the liquid/air interface which was then traced with the in-built 'Canny' edge detection routine distributed with MATLAB®. With the liquid/air interface identified, the filament

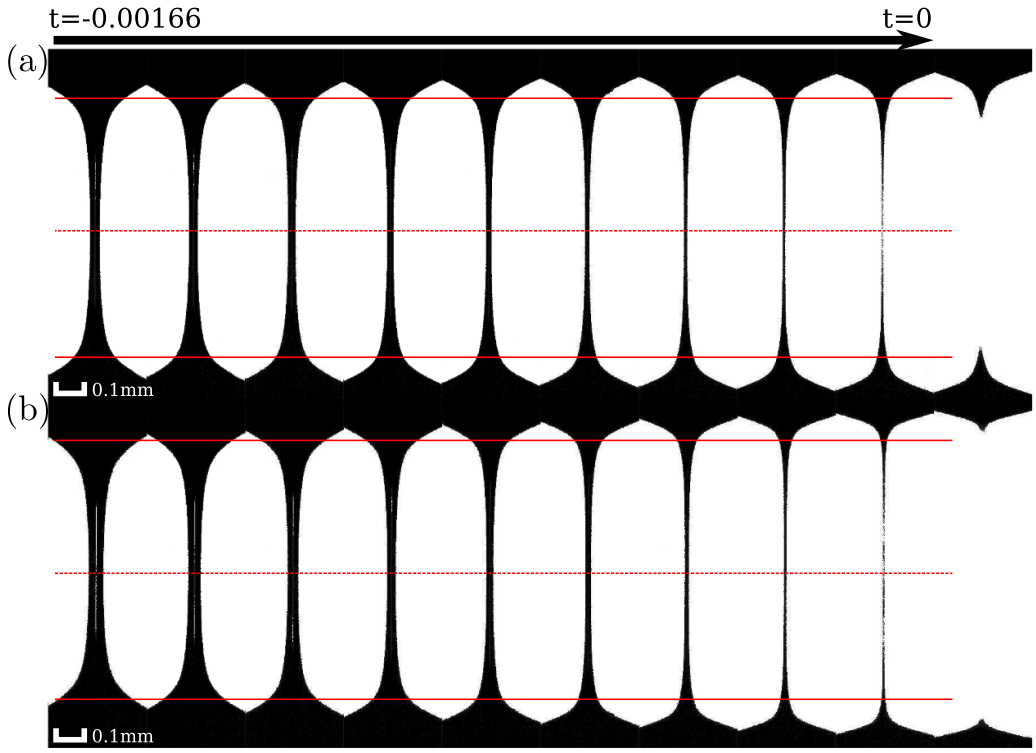

Figure 1. Filament profiles for capillary thinning experiments for (a) 95:5% and (b) 90:10% by weight glycerine-water mixture, respectively. Dashed red lines represent nominal filament mid-height. Solid red lines indicate boundary of 'virtual' laser micrometer with 1 mm thickness.

radius evolution can easily be extracted from the image sequences.

For this study, we have performed experiments on glycerine-water solutions with concentrations of 95:5 and 90:10 wt.% and one shear-thinning power-law fluid, a volume concentration $\phi = 0.3$ vol% aqueous graphene-oxide (GO) solution which we have reported previously in [33]. For these relatively low viscosity solutions, we forgo the standard 'step-stretch' protocol and adopt the so-called 'SRM' which was initially introduced by Campo-Deaño and Clasen [27] to probe the extensional viscosity of elastic fluids with ultra-short relaxation times. With this method, the liquid bridge is instead brought close its stability limit before the end-plates are driven apart at a very slow velocity ($\sim$0.2 mm s^{-1}) to initiate the filament breakup process in lieu of applying a step-stretch. The SRM was developed to minimize the effect of inertia on low viscosity elastic fluids [27] and we adopt the methodology even though our fluids are essentially inelastic.

3. Newtonian fluid validation experiments

To establish the accuracy and repeatability of our experimental setup we first conducted measurements on Newtonian fluids with a known response. As Newtonian reference cases, capillary breakup experiments using the SRM [27] were performed on 95:5 and 90:10 wt.% glycerine-water solutions with nominal shear viscosities of $\eta_S = 384$ mPa s and $\eta_S = 213$ mPa s, respectively. Shear viscosities of the glycerine-water mixtures were measured at $T = 20$ °C on an Anton Paar MCR302 using a cone-and-plate geometry (plate diameter $D_{\text{plate}} = 60$ mm and cone angle 2°). Each glycerine-water solution was tested five times in the CaBER to check repeatability. Example image sequences of the filaments near breakup are shown in figure 1 (thresholded to increase the contrast between foreground and background) where we treat the breakup time as $t = 0$. We observe that the filaments break at their mid-height as expected at these sufficiently high viscosities, where capillarity is solely balanced by viscosity and inertia remains unimportant. The time evolution of the minimum filament diameter of the two glycerine-water solutions near breakup are plotted in figure 2 and the collapse of the data for all runs indicates very good repeatability. As the fluid filament undergoes self-thinning, it approaches the similarity solution proposed by [3] who predicts that the filament diameter decreases linearly with time (in the absence of inertia) according to

$$R_{\text{mid}}(t) = 0.0709\frac{\sigma}{\eta_S}(t_c - t), \tag{5}$$

where t_c is the filament breakup time and from which one can extract the shear viscosity η_S and/or surface tension σ with only an independent measure of the other. The evolution equation (5) can only apply in the late stages of thinning as the filament must become sufficiently slender to: (1) approach an ideal axial cylinder and (2) for gravitational effects to be negligible. McKinley and Tripathi [2] demonstrate that in the early stages of thinning of a Newtonian filament the gravitational

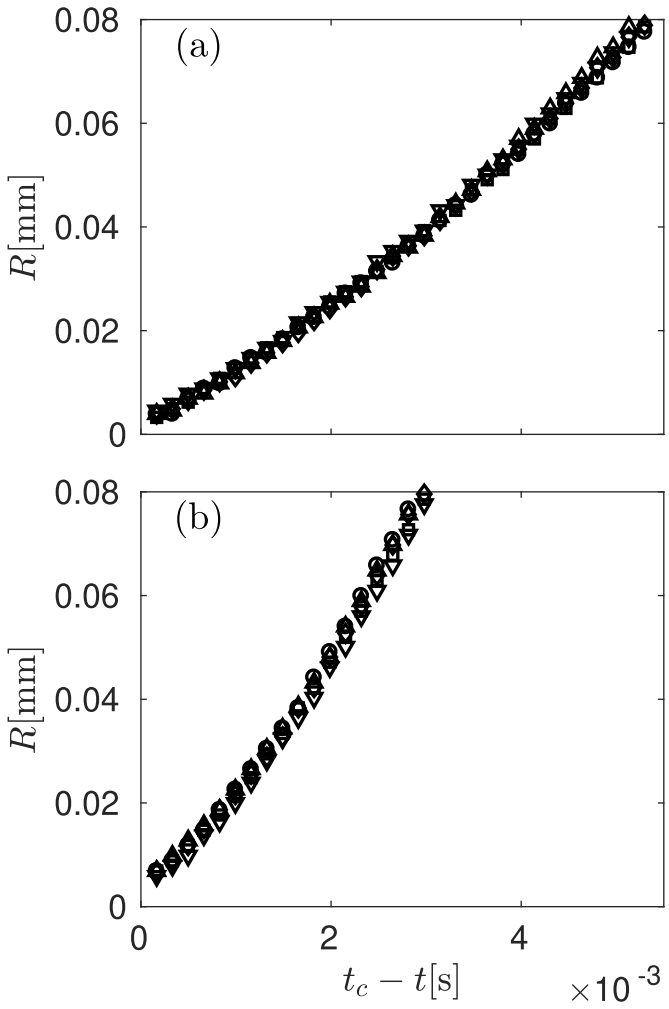

Figure 2. Time evolution of filament mid-height radius close to break up for two glycerine-water solutions corresponding to figure 1. Symbols represent individual measurements indicating good repeatability. Nominal shear viscosity measured at $T = 20\ ^{\circ}\mathrm{C}$ of (a) $\eta_S = 384$ mPa s and (b) $\eta_S = 213$ mPa s.

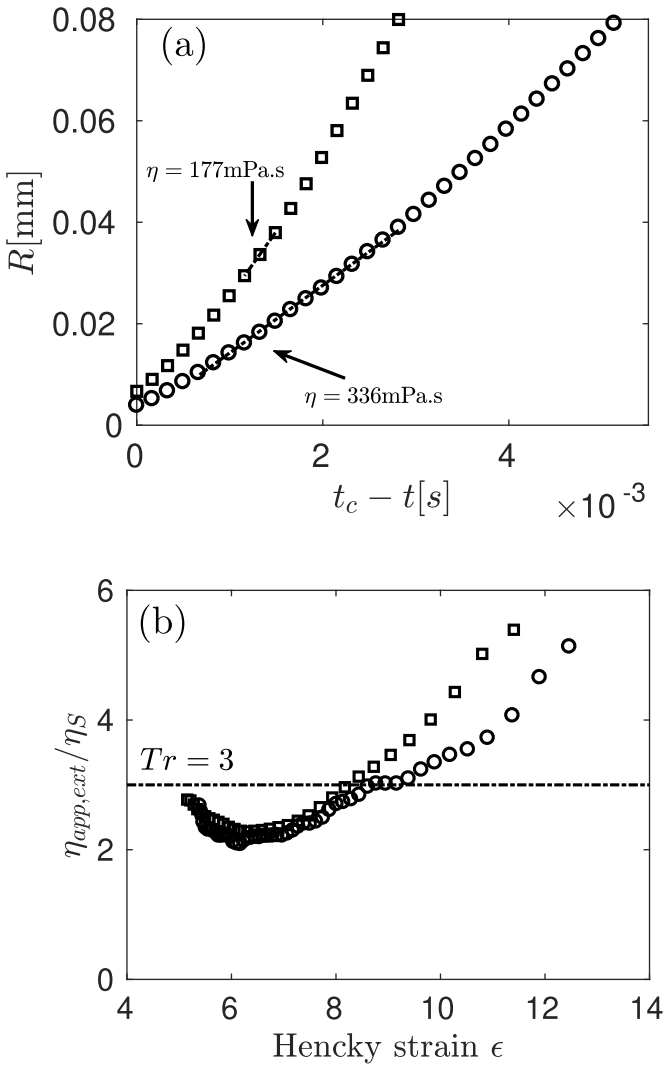

Figure 3. (a) Averaged filament mid-height radius evolution over five measurements. Shear viscosities back calculated by fitting the thinning rate. (b) Apparent extensional viscosity ($Tr = \eta_{\mathrm{app,ext}}/\eta_S$) versus Hencky strain, ϵ.

effects are not negligible and that the filament undergoes 'gravitational drainage'. Gravity forces only become relatively unimportant when the Bond number $B_0 = \rho g R^2/\sigma$ becomes much less than unity; where $g = 9.81\ \mathrm{m\,s^{-2}}$ is the gravitational acceleration. To provide a somewhat less subjective measure of 'late stages of thinning' we follow [2] and consider gravitational forces to the negligible for $B_0 < 0.1$ which suggests that the similarity solution of [3] is applicable for diameter ranges of

$$2R_{\mathrm{mid}}(t) \leqslant \sqrt{\frac{0.1\sigma}{\rho g}}. \tag{6}$$

A more recent study by Verbeke *et al* [34] shows that the length of the filament is also an important consideration in determining the applicable limits of equation (5). The authors in that study introduce an Ohnesorge number based on the length of the filament:

$$Oh_L = \frac{\eta_S}{\sqrt{\sigma\rho L}}, \tag{7}$$

where L is the axial length scale. They show via dimensional analysis that a critical radius R_{crit} for the transition from viscous scaling [3] to inertio-viscous scaling [35] is given by

$$\frac{R_{\mathrm{crit}}}{L} = \frac{0.11}{Oh_L^2}. \tag{8}$$

R_{crit} thus sets the lower limit for the applicability of the evolution equation (5). An upper limit is set by the slenderness assumption, i.e. $R/L << 1$. Estimating an axial length scale $L = 0.4$ mm from inspection of figure 1 yields an upper limit of $R_{up} = 40$ μm, (assuming $L \geqslant 10 \times R_{up}$ to satisfy the slenderness assumption) which satisfies equation (6), and lower limits of $R_{\mathrm{crit}} \approx 10$ μm and ≈30 μm for the glycerine-water solutions of 95: 5 and 90:10 wt.%, respectively.

The data presented in figure 2 is now averaged and plotted in figure 3(a) along with a linear regression to the data over

the range outlined above. The radii values here are extracted at filament mid-height. The gradient of the regression fit can be used to determine the capillary velocity (σ/η_S) from which we can obtain the shear viscosity and compare this value with that from an independent measurement to ascertain the accuracy of our experimental setup. Surface tensions σ for the 95: 5 and 90:10 wt.% glycerine solutions are $\sigma = 63.1$ mNm and $\sigma = 63.9$ mNm, respectively [36]. Hence, we calculate from linear regression, shear viscosities of $\eta_S = 336$ mPa s and $\eta_S = 177$ mPa s for our 95: 5 and 90:10 wt.% solutions, respectively, which is within ≈15% of the value measured from shear rheometry. The discrepancy between shear viscosities measured directly and obtained from linear regression can likely be explained by the hygroscopic nature of glycerine. As glycerine is exposed to air, it continues to absorb moisture thus lowering the concentration leading to a subsequent decrease in viscosity over time as noted by [2].

The apparent extensional viscosity $\eta_{\text{app,ext}}$ (calculated from equation (3)) is normalised by shear viscosity η_S obtained from linear regression to give the so-called Trouton ratio, $Tr = (\eta_{\text{app,ext}}/\eta_S)$ which we plot as a function of Hencky strain, ϵ (estimated using equation (4)) in figure 3(b). Interestingly, we do not observe an elongated plateau at $Tr = 3$ as expected for a Newtonian fluid, although a small plateau exists for the 95:5 wt.% solution between Hencky strains of $8.5 \lesssim \epsilon \lesssim 9$. This is likely due to filament curvature; largely unavoidable when using the slow retraction method which, by virtue of the technique, essentially sets up the *shortest* possible filament for capillary thinning and breakup. However, even given these considerations, we show that the calculated Trouton ratio has an *average* value of $Tr = 3 \pm 1$ as expected for a Newtonian fluid. That the Trouton ratio (calculated using shear viscosity from linear regression) is equal to 3 within the observation window where viscous and capillary forces are in balance is reassuring and supports our conjecture that the difference in shear viscosity obtained from direct measurement and linear regression is due to the hygroscopic nature of glycerine. Overall, our Newtonian validation experiments agree very well with theory and observations previously reported in the literature.

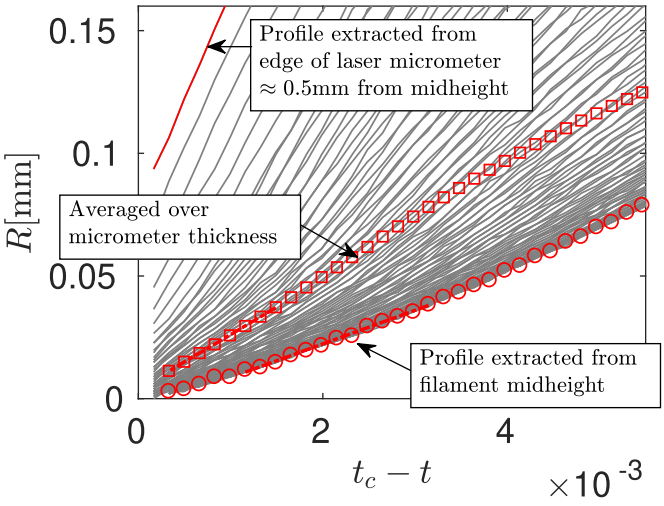

Figure 4. Time evolution of measured filament radius. Grey lines indicate every fifth radius profile extracted at different heights within the thickness of the laser micrometer (see figure 1). Red squares indicate the average radius from the 'virtual' laser micrometer. Red circles represent the radius profile extracted at filament mid-height.

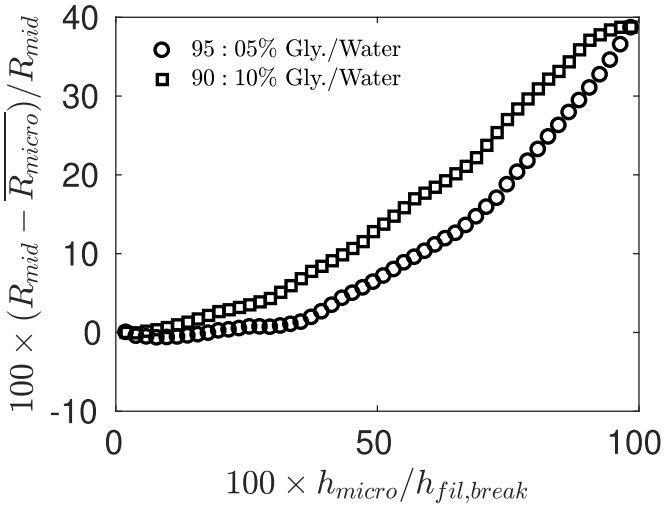

Figure 5. Percentage errors due to averaging over finite thickness of the laser micrometer shown as a function of filament height.

4. Errors due to averaging over finite thickness

We now consider a 'virtual' laser micrometer with thickness of 1 mm (as indicated by red solid lines in figure 1). Filament profiles from a single measurement are extracted from the image sequence over an axial height of 1 mm with every fifth profile shown in grey in figure 4. Shown together in figure 4 is the averaged filament radius profile measured using the 'virtual' laser micrometer, $\overline{R_{\text{micro}}}$, in red squares and the profile corresponding to filament nominal mid-height R_{mid} in red circles. Clearly, significant errors can arise from averaging over the finite thickness of the laser micrometer. Following the same procedure to back calculate shear viscosity as outlined in section 3, pixel lines extracted from high-speed imaging at filament mid-height yielded a shear viscosity of $\eta_S = 327$ mPa s which is within 3% of the value obtained in section 3 (which was calculated from the averaged thinning profile). Performing the same procedure on the filament evolution extracted using the 'virtual' laser micrometer yielded a shear viscosity of $\eta_S = 200$ mPa s, which is a difference of 40% from the value extracted at filament midheight. We can reduce (or increase) the thickness of our 'virtual' laser micrometer, h_{micro} by reducing (or increasing) the number of pixel lines that we extract from our high-speed images. Normalising h_{micro} by the filament height immediately prior to breakup $h_{\text{fil,break}}$ we can assess the error due to averaging over micrometer thickness as a function of filament height relative to the measured radius evolution at filament mid-height (figure 5). We find for these relatively short Newtonian viscous filaments, which are nominally symmetric about the mid-height, that the errors are small ($< \pm 1\%$) when the micrometer thickness is less than ≈20% of

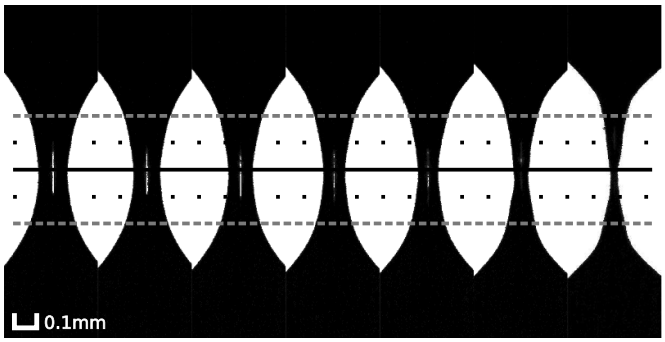

Figure 6. Filament evolution for $\phi = 0.3$ vol% GO solution immediately prior to breakup. Images shown have time step of $\Delta t \approx 0.0331$ ms. Solid black line indicates filament mid-height. Dotted black lines represent deviations from filament mid-height of $x_{\text{mid}} \pm 0.1$ mm and dashed grey lines a deviation of $x_{\text{mid}} \pm 0.2$ mm.

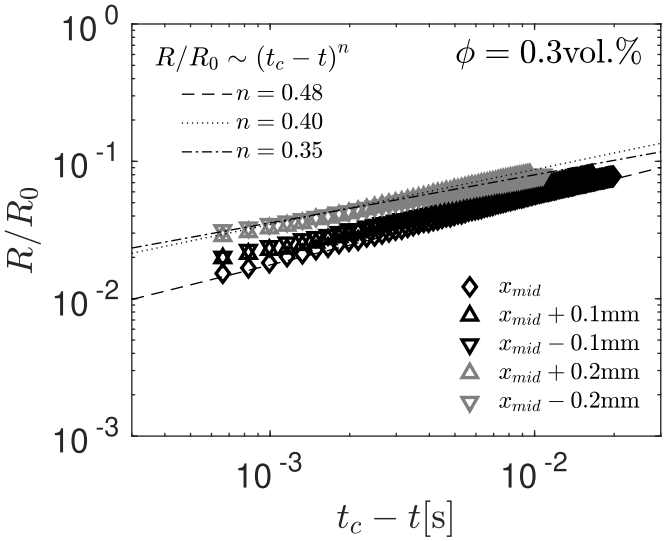

Figure 7. Filament evolution profiles for GO with concentration $\phi = 0.3$ vol% extracted from high-speed images at different axial locations. ($\diamond$):location of breakup; black ($\triangle$): 0.1 mm above breakup; grey ($\triangle$): 0.2 mm above breakup; black ($\triangledown$): 0.1 mm below breakup and grey ($\triangledown$): 0.2 mm below breakup.

the filament height at breakup and increase rapidly to ≈10% when the micrometer thickness reaches ≈50% of filament height at breakup, with the errors higher for the 90:10 wt.% solutions due to a higher filament axial curvature.

5. Errors due to axial misalignment

In many deformation-thinning yield-stress fluids, the axial location of filament breakup is often not known *a priori* [21]. Here, we consider briefly the effect of axial misalignment of the laser micrometer in relation to the location of ultimate filament breakup. Again, we consider a 'virtual' laser micrometer by extracting pixel lines from high-speed images. In this example, we report results of capillary breakup experiments performed using the SRM on aqueous solutions of GO at a volume concentration of $\phi = 0.3$ vol%. Images of the filament-thinning prior to breakup are shown in figure 6,

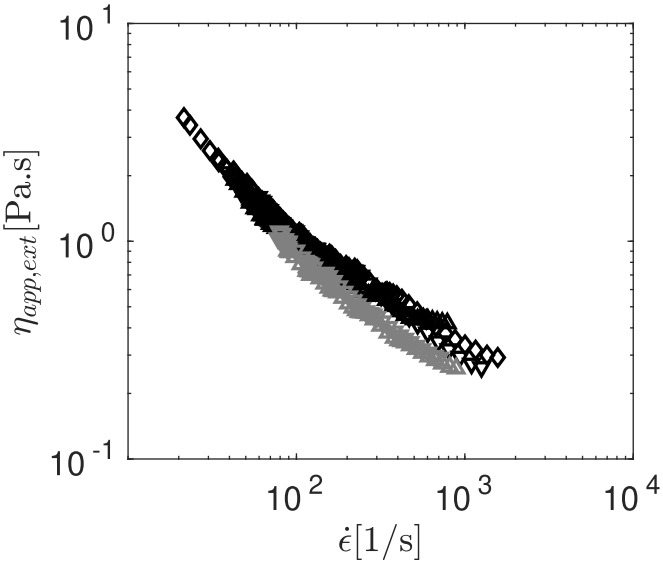

Figure 8. Apparent extensional viscosity $\eta_{\text{app,ext}}$ as a function of strain rate $\dot{\epsilon}$ calculated from evolution shown in figure 7 (using equations (3) and (1), respectively).

where horizontal lines represent the filament mid-height x_{mid} (solid line) and deviations of $x_{\text{mid}} \pm 0.1$ mm (dotted lines) and $x_{\text{mid}} \pm 0.2$ mm (dashed lines). We have shown previously in [33] that GO solutions at this concentration are shear-thinning, power-law fluids with a power-law index of $m = 0.44$ measured using steady-shear rheometry. The capillary thinning of power-law fluids can be represented as [37]

$$\frac{R(t)}{R_0} = \Phi(n)\frac{\sigma}{K}(t_c - t)^n, \tag{9}$$

where K is the consistency factor, $\Phi(n)$ is a numerical constant and n is the power-law exponent. We find that when extracting the filament profile at the actual axial location of ultimate breakup, the power-law index n extracted by fitting the thinning profile using equation (9) is $n = 0.48$, very close to the value obtained from shear rheometry. When deviating from the axial location of break up by $x_{\text{mid}} \pm 0.1$ mm and $x_{\text{mid}} \pm 0.2$ mm (shown as black and grey triangles in figure 7, with upwards facing triangles indicative of a positive deviation and downwards facing triangles indicative of a downwards deviation), we find the extracted filament-thinning profiles to be significantly different with power law indices of $n = 0.35$ for a $x = 0.2$ mm upshift and $n = 0.40$ for a $x = 0.2$ mm deviation downwards. That the fitted power-law indices extracted from thinning profiles that are equidistant from the breakup location are not the same indicates that the filament is not symmetric, further highlighting the need for imaging in capillary breakup experiments.

The apparent extensional viscosity $\eta_{\text{app,ext}}$ (equation (3)) shown as a function of strain rate $\dot{\varepsilon}$ (equation (1)) for the data displayed in figure 7 is shown in figure 8. Here, symbols retain their meaning from figure 7. We find that for axial misalignments of $x = \pm 0.1$ mm errors can reach up to ≈15% and with

displacements of $x = 0.2$ mm, the apparent extensional viscosity can be in error by up to ≈35% at a given deformation rate for our aqueous GO solution at $\phi = 0.3$ vol%.

6. Conclusions

With two simple example experiments, we have highlighted the need for high-speed imaging in capillary breakup extensional rheometry rather than using a laser micrometer with a finite thickness as many previous studies have done [6–19].

Using a 'virtual' laser micrometer, we show that errors induced by averaging over the finite thickness of a laser micrometer can be up to 40% in the case of short, Newtonian viscous filaments like those tested here. We show, also, that for a deformation-thinning power-law fluid the impact of laser micrometer misalignment with the location of filament breakup can lead to significant errors in the apparent extensional viscosity. Of course, the errors induced in both examples considered are due to filament curvature, which only further reinforces the need for imaging in these experiments.

So far we have tested only viscous and shear-thinning (i.e. inelastic) fluids, and we do expect that errors for viscoelastic fluid filaments (tested within the same geometrical parameters) to be far less pronounced due to their natural inclination to be more cylindrical. However, there will still be non-negligible errors associated with averaging over the thickness of the laser micrometer and micrometer axial misalignment in the event that the laser micrometer thickness (relative to the filament height) and location cause the measurement of the filament evolution to be taken within the end-drops of the liquid bridge. Determining the critical ratio of filament height to micrometer thickness beyond which the errors outlined in this paper would become negligible could be achieved by using the standard CaBER step-stretch protocols to generate filaments of different heights. However, the curvature and shape of the filament profiles, which to a large extent drives the errors observed here, appear to also depend on the type of fluid tested (i.e. viscous, elastic, deformation-thinning, yield-stress) and a full exploration that parameter space is beyond the scope of the current paper but the subject of future work. For a practical 'rule-of-thumb', our current results (for Newtonian filaments) suggest that, in the absence of axial misalignment, the errors due to averaging over the laser micrometer thickness are negligible ($\leqslant$1%) when the laser micrometer thickness is less than ≈20% of the filament height (with this limit increasing for viscoelastic fluids which tend to be more cylindrical).

Whilst long, slender, nominally-cylindrical filaments (typically associated with highly-elastic fluids) will not likely suffer from the errors outlined here, the push to measure at lower viscosities necessitates measurements on short filaments (i.e. using the SRM protocol in the standard CaBER device, or the 'DoS' rheometer [29]) where the errors outlined in this paper may play a significant role, thus further emphasizing the need for high-speed imaging in CaBER measurements (especially when employing SRM and DoS techniques to probe fluids with low viscosity and ultra-short relaxation times).

Furthermore, the filament evolution of many yield stress fluids, regardless of testing protocol (i.e. either step-stretch or SRM), exhibit conical tapering prior to breakup where the axial location of breakup is typically not known *a priori* (see, for example: [21, 22]). In the case of these fluids, imaging techniques would be a must when attempting to extract material properties from capillary breakup experiments.

Data availability statement

The data that support the findings of this study are available upon reasonable request from the authors.

Acknowledgment

R J P would like to thank the EPSRC for the award of a Fellowship under Grant No. EP/M025187/1.

ORCID iDs

Henry C-H Ng https://orcid.org/0000-0003-4926-7622
Robert J Poole https://orcid.org/0000-0001-6686-4301

References

[1] Bazilevsky A V, Entov V M and Rozhkov A N 1990 Liquid filament microrheometer and some of its applications *Third European Rheology Conf. and Golden Jubilee Meeting of the British Society of Rheology*, ed D R Oliver (Dordrecht: Springer) (https://doi.org/10.1007/978-94-009-0781-2_21)
[2] McKinley G H and Tripathi A 2000 How to extract the Newtonian viscosity from capillary breakup measurements in a filament rheometer *J. Rheol.* **44** 653–70
[3] Papageorgiou D T 1995 On the breakup of viscous liquid threads *Phys. Fluids* **7** 1529–44
[4] Anna S L and McKinley G H 2001 Elasto capillary thinning and breakup of model elastic liquids *J. Rheol.* **45** 115–38
[5] Entov V M and Hinch E J 1997 Effect of a spectrum of relaxation times on the capillary thinning of a filament of elastic liquid *J. Non-Newton. Fluid Mech.* **97** 31–53
[6] Anna S L, McKinley G H, Nguyen D A, Sridhar T, Muller S J, Huang J and James D F 2001 An interlaboratory comparison of measurements from filament-stretching rheometers using common test fluids *J. Rheol.* **45** 83–114
[7] Clasen C, Plog J P, Kulicke W-M, Owens M, Macosko C, Scriven L E, Verani M and McKinley G H 2006 How dilute are dilute solutions in extensional flows? *J. Rheol.* **50** 849–81
[8] Bhardwaj A, Miller E and Rothstein J P 2007 Filament stretching and capillary breakup extensional rheometry measurements of viscoelastic wormlike micelle solutions *J. Rheol.* **51** 693–719
[9] Miller E, Clasen C and Rothstein J P 2009 The effect of step-stretch parameters on capillary breakup extensional rheology (CaBER) measurements *Rheol. Acta* **48** 625
[10] Haward S J, Sharma V, Butts C P, McKinley G H and Rahatekar S S 2012 Shear and extensional rheology of cellulose/ionic liquid solutions *Biomacromolecules* **13** 1688–99
[11] Khandavalli S and Rothstein J P 2014 Extensional rheology of shear-thickening fumed silica nanoparticles dispersed in an aqueous polyethylene oxide solution *J. Rheol.* **58** 411–31

[12] Galindo-Rosales F J, Segovia-Gutiérrez J P, Pinho F T, Alves M A and Vicente J d 2015 Extensional rheometry of magnetic dispersions *J. Rheol.* **59** 193–209
[13] Piermaría J, Bengoechea C, Abraham A G and Guerrero A 2016 Shear and extensional properties of kefiran *Carbohydrate Polym.* **152** 97–104
[14] Vadodaria S S and English R J 2016 Extensional rheometry of cellulose ether solutions: flow instability *Cellulose* **23** 339
[15] Lundahl M J, Berta M, Ago M, Stading M and Rojas O J 2018 Shear and extensional rheology of aqueous suspensions of cellulose nanofibrils for biopolymer-assisted filament spinning *Eur. Polym. J.* **109** 367–78
[16] Azad M S and Trivedi J J 2019 Novel viscoelastic model for predicting the synthetic polymer's viscoelastic behavior in porous media using direct extensional rheological measurements *Fuel* **235** 218–26
[17] Andrade R J E, Jacob A R, Galindo-Rosales F J, Campo-Deaño L, Huang Q, Hassager O and Petekidis G 2020 Dilatancy in dense suspensions of model hard-sphere-like colloids under shear and extensional flow *J. Rheol.* **64** 1179–96
[18] Surber G, Jaros D and Rohm H 2020 Shear and extensional rheology of acid milk gel suspensions with varying ropiness *J. Texture Stud.* **51** 111–9
[19] Du J, Ohtani H, Owens C E, Zhang L, Ellwood K and McKinley G H 2021 An improved capillary breakup extensional rheometer to characterize weakly rate-thickening fluids: applications in synthetic automotive oils *J. Non-Newton. Fluid Mech.* 104496
[20] Vadillo D C, Mathues W and Clasen C 2012 Microsecond relaxation processes in shear and extensional flows of weakly elastic polymer solutions *Rheol. Acta* **51** 755–69
[21] Martinie L, Buggisch H and Willenbacher N 2013 Apparent elongational yield stress of soft matter *J. Rheol.* **57** 627–46
[22] Valette R, Hachem E, Khalloufi M, Pereira A S, Mackley M R and Butler S A 2019 The effect of viscosity, yield stress and surface tension on the deformation and breakup profiles of fluid filaments stretched at very high velocities *J. Non-Newton. Fluid Mech.* **263** 130–9
[23] Mathues W, McIlroy C, Harlen O G and Clasen C 2015 Capillary breakup of suspensions near pinch-off *Phys. Fluids* **27** 093301
[24] Lang C, Hendricks J, Zhang Z, Reddy N K, Rothstein J P, Lettinga M P, Vermant J and Clasen C 2019 Effects of particle stiffness on the extensional rheology of model rod-like nanoparticle suspensions *Soft Matter* **15** 833–41
[25] Rodd L E, Scott T P, Cooper-White J J and McKinley G H 2005 Capillary break-up rheometry of low-viscosity elastic fluids *Appl. Rheol.* **15** 12–27
[26] Vadillo D C, Tuladhar T R, Mulji A C, Jung S, Hoath S D and Mackley M R 2010 Evaluation of the inkjet fluid's performance using the 'cambridge trimaster' filament stretch and break-up device *J. Rheol.* **54** 261–82
[27] Campo-Deaño L and Clasen C 2010 The slow retraction method (SRM) for the determination of ultra-short relaxation times in capillary breakup extensional rheometry experiments *J. Non-Newton. Fluid Mech.* **165** 1688–99
[28] Dinic J, Zhang Y, Jimenez L N and Sharma V 2015 Extensional relaxation times of dilute, aqueous polymer solutions *ACS Macro Lett.* **4** 804–8
[29] Dinic J, Jimenez L N and Sharma V 2017 Pinch-off dynamics and dripping-onto-substrate (DoS) rheometry of complex fluids *Lab Chip* **17** 460–73
[30] Dinic J, Biagioli M and Sharma V 2017 Pinch-off dynamics and extensional relaxation times of intrinsically semi-dilute polymer solutions characterized by dripping-onto-substrate rheometry *J. Polym. Sci.* B **55** 1692–704
[31] Jimenez L N, Dinic J, Parsi N and Sharma V 2018 Extensional relaxation time, pinch-off dynamics and printability of semidilute polyelectrolyte solutions *Macromolecules* **51** 5191–208
[32] Sur S and Rothstein J 2018 Drop breakup dynamics of dilute polymer solutions: effect of molecular weight, concentration and viscosity *J. Rheol.* **62** 1245–59
[33] Ng H C-H, Corker A, García-Tuñón E and Poole R J 2020 GO CaBER: capillary breakup and steady-shear experiments on aqueous graphene oxide (GO) suspensions *J. Rheol.* **64** 81–93
[34] Verbeke K, Formenti S, Vangosa F B, Mitrias C, Reddy N K, Anderson P D and Clasen C 2020 Liquid bridge length scale based nondimensional groups for mapping transitions between regimes in capillary break-up experiments *Phys. Rev. Fluids* **5** 051901
[35] Eggers J 1993 Universal pinching of 3d axisymmetric free-surface flow *Phys. Rev. Lett.* **71** 3458–60
[36] 1963 *Physical Properties of Glycerine and Its Solutions* (Glycerine Producers' Association)
[37] McKinley G H 2005 Visco-elasto-capillary thinning and breakup of complex fluids *Br. Soc. Rheol.* 1–49, 01